UNIVERSITÉ CATHOLIQUE DE LOUVAIN

Study of the stress relieve heat-treatment of additively manufactured AlSi10Mg alloy:

Influence on microstructure and mechanical properties

Dissertation presented by

David DISPAS *and* Arthur BOUILLOT

for obtaining the Master's degree in

Mechanical Engineering *and* Chemical and Materials Engineering

at Ecole Polytchnique de Louvain (EPL)

Supervisor: Aude SIMAR

Readers: Laurent DELANNAY, Anne MERTENS, Camille VAN DER REST

Academic year 2017-2018

‘Citation stylée.’

Mec cool

Acknowledgements

Blablabla. blabla. bla.

Contents

1 Introduction 1

2 State of the art 3
  2.1 Selective laser melting technology . . . 3
  2.2 AlSi10Mg alloy . . . 5
  2.3 Fabrication process parameters . . . 5
  2.4 Post treatments . . . 8

3 Materials and methods 9
  3.1 Powder follow-up . . . 9
    3.1.1 Sieving . . . 9
    3.1.2 Grain size and distribution . . . 9
    3.1.3 Composition . . . 9
  3.2 Fabrication process parameters . . . 9
  3.3 Heat treatments . . . 10
  3.4 Characterisation . . . 11
    3.4.1 Density . . . 11
      Hydrostatic weighing . . . 11
      Relative optical density image analysis . . . 12
    3.4.2 Microscopy . . . 13
      Scanning electron microscopy . . . 13
      Optical microscopy . . . 13
    3.4.3 Composition . . . 13
    3.4.4 Mechanical properties . . . 13
      Hardness test . . . 13
      Traction test . . . 14

4 Results 15
  4.1 Parameters optimisation . . . 15
  4.2 Reproducibility . . . 15
  4.3 Powder ageing . . . 15
    4.3.1 Grain size and distribution . . . 15
    4.3.2 Composition . . . 15
      Fresh powder . . . 15
      Recycled powder . . . 15
  4.4 Heat treatments . . . 15
  4.5 Mechanical testing . . . 15

5 Discussion 17
  5.1 Parameters optimisation . . . 17
  5.2 Reproducibility . . . 17
  5.3 Powder ageing . . . 17
    5.3.1 Grain size and distribution . . . 17

5.3.2 Composition 17
5.4 Density measures assessments 17
5.5 Heat treatment optimisation 17

6 Conclusion **19**

A Batches fabrication details **21**
A.1 Process parameters 21
A.2 Specimens positioning, fabrication orders and sintering times 21
A.2.1 Batch X200-171024 21
A.2.2 Batch X200-180109 21
A.2.3 ...Other batches 21

Bibliography **25**

List of Figures

2.1 Selective laser melting technology principle 3
2.2 (a)Research publications on SLM of ceramics, composites and all materials types combined. (b)Research publications on SLM of different metallic materials 4
2.3 Parameters involved in SLM 5
2.4 Process window for SLM of AlSi10Mg, based on the top view of single track scans 6
2.5 Process window for SLM of AlSi10Mg, based on the front view of single track scans 6
2.6 Schematic representation of scanning strategies commonly used in LSM (a) unidirectional long scan track; (b) bi-directional long scan track, and (c) islands 7
2.7 Samples (static tensile) built in different directions: (a) 0°, (b) 45°, and (c) 90° 8

3.1 ProX DMP 200 printer 10
3.2 Melt pool contours with and without laser compensation (exaggeration) 11
3.3 Laser compensations as a function of the scanning speed (as recommended by the manufacturer) 12
3.4 RODIA procedure for specimen X200-180319-cub 1: (a) Original picture of polished section (b) Whole surface isolation with *ImageJ* (c) Porosities isolation with *ImageJ*. 13
3.5 Schematization of the Vickers harness test 14

A.1 Dimensions notations for (a) cubic specimens (b) cylindrical specimens 21
A.2 Specimens positions, order of fabrication and sintering times for batch X200-171024 22
A.3 Photography of the manufacturing plate after completion of the fabrication of batch X200-171024 22

List of Tables

3.1 Polishing routine for Al-Si alloys 13
4.1 Composition of recycled AlSi10Mg powder as a function of the date . 15
A.1 Process parameters used for the specimens manufacturing 23

List of Abbreviations

AM	**A**dditive **M**anufacturing
CAD	**C**omputer **A**ided **D**esign
DMLS	**D**irect **M**etal **L**aser **S**intering
DMP	**D**irect **M**etal **P**rinter
ICP	**I**nductively **C**oupled **P**lasma
RODIA	**R**elative **O**ptical **D**ensity **I**mage **A**nalysis
SEM	**S**canning **E**lectron **M**icroscope
SLM	**S**elective **L**aser **M**elting

Symbols

D_a	Average particle size	$[\mu m]$
E_d	Volumetric energy density	$[\frac{J}{mm^3}]$
h	Hatch space	$[\mu m]$
H_v	Vickers hardness	$[HV]$
P	Laser power	$[W]$
p_{O_2}	Oxygen pressure	$[mbar]$
t	Layer thickness	$[\mu m]$
v_s	Scanning speed	$[\frac{mm}{s}]$
W_a	Specimen dry weight	$[g]$
W_w	Specimen underwater weight	$[g]$
ϵ_f	Strain at fracture	[-]
$\phi_{99\%}$	Laser spot size at the 99% contour	$[\mu m]$
λ	Laser wavelength	$[nm]$
ρ_a	Apparent density	$[\frac{g}{cm^3}]$
$\rho_{a,rel}$	Apparent relative density	$[-]$
ρ_w	Water density	$[\frac{g}{cm^3}]$
ρ_{rel}	Relative density	$[-]$
σ_u	Ultimate tensile stress	$[MPa]$

Nous dédions ce travail à nos familles et amis

Chapter 1

Introduction

This is, with the concluding chapter, a significant portion of memory. This should especially present the context and objectives of the work. Generally, the memory structure (content of chapters) is briefly exposed

Chapter 2

State of the art

2.1 Selective laser melting technology

Selective laser melting (SLM) - also referred to as direct metal laser sintering (DMLS) - is an additive manufacturing (AM) technique making use of a high power-density laser that locally melts powder materials.When a layer of powder has been melted, a new layer is spread on top of the previous one, and is in turn melted, in order to progressively build a 3D object. The technique is illustrated on figure 2.1 [12]. The materials used include mostly metals but also ceramics and composites. Parts to build must first be drawn in a computer-aided design (CAD) software and broken down in 2D slices, each one corresponding to a powder layer. During the process, the oxygen pressure p_{O_2} must be kept low to prevent the oxidation of the metal. A shielding gas - such as argon - is thus used to fill the build chamber at all time, while p_{O2} is monitored.

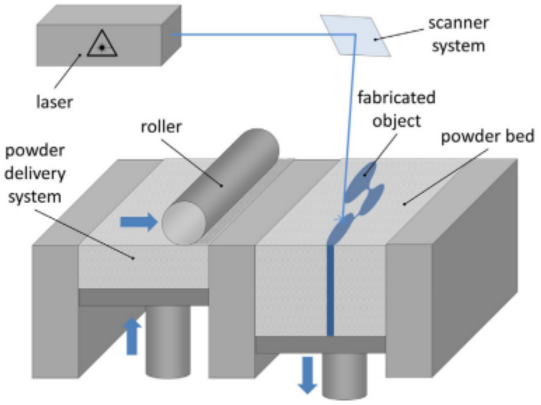

FIGURE 2.1: Selective laser melting technology principle (from Leitz et al, 2016).

LSM is still a young technology. Its popularity only increased significantly over the last decade, as depicted by figures 2.2 (a) and (b). Works concerning AlSi10Mg began to emerge noticeably in 2014. The technique usage spread rapidly in many sectors: biomedical, heat exchangers, aerospace and automotive - to name just a few [24]. This is due to the numerous appeals of SLM compared to the other technologies, including:

- Geometrical flexibility: parts can be designed with thin walls or even with hidden cavities and/or channels. This offers promising prospects regarding light-weight potentials for parts solicited mechanically [14];
- Increased reliability of the parts [8];
- Reduced equipment costs [9];
- Better operational efficiency: the fabrication is quick and easy which reduces time-to-market as well as assembly times and capital tied up in stocks [9];
- Individual production facilitation [8];
- Reduced material waste and better energy usage: the process is environmentally friendly as a whole [8].

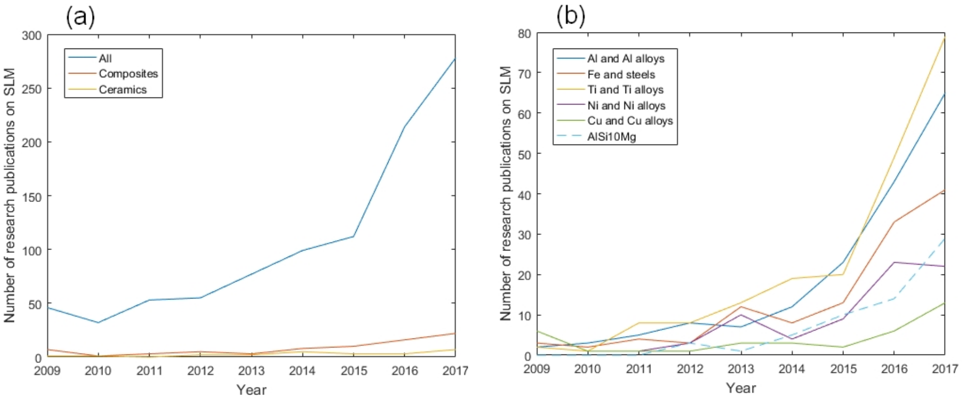

FIGURE 2.2: (a)Research publications on SLM of ceramics, composites and all materials types combined. (b)Research publications on SLM of different metallic materials. Data are derived from the research publications on SLM, LaserCusing and DMLS existing on ScienceDirect website.

The properties of parts produced trough SLM stem from the coupled effects of a great deal of parameters (see figure 2.3) [3]. Results are very sensitive to their variations. The process parameters must thus be monitored thoroughly. This complicates the search for their optimisation, still not fully resolved for aluminium alloys.

In recent years, works aiming at facing this challenge multiplied. The minimisation of the porosity is at the center of attention. It is indeed closely related to the quality of the mechanical properties. As porosity contributes to lowering the load-bearing surface, it reduces the apparent material strength. It was also observed to have a critical influence on the fatigue life of the produced parts. Their lifetime is especially diminished if the values of pores amount and size go beyond a certain threshold [5]. Studies investigating the effects of various parameters on the AlSi10Mg fabrication trough SLM abound in the literature.

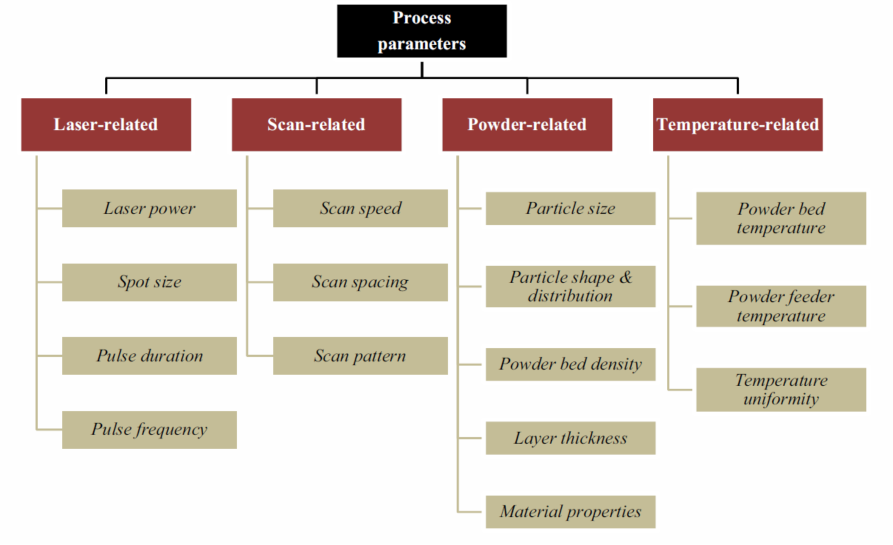
Process parameters
Laser-related
Scan-related
Powder-related
Temperature-related
Laser power
Spot size
Pulse duration
Pulse frequency
Scan speed
Scan spacing
Scan pattern
Particle size
Particle shape & distribution
Powder bed density
Layer thickness
Material properties
Powder bed temperature
Powder feeder temperature
Temperature uniformity

FIGURE 2.3: Parameters involved in SLM (from Aboulkhair et al, 2014).

2.2 AlSi10Mg alloy

Parler de l'AlSi10Mg; quel est l'interet de travailler avec? Difficultés? (reflectivité etc).. Qu'est ce qui existe en coulé, forgé etc
Microstructure homogène, diagramme de phase

2.3 Fabrication process parameters

Let us now investigate the influence of the parameters on the process. The analysis of the paired impacts of the laser power P and scan speed v_s provides a first insight. As depicted by figures 2.4 and 2.5, low P and high v_s lead to an insufficient energy input to melt the powder and re-melt the substrate, which causes the formation of droplets [11] . The opposite leads to good penetration but also to distortions and irregularities. A trend to use both high P and v_s rose in accordance with these findings. Doing so has the advantage to increase productivity. However, it also has multiple downsides including a decrease of the surface quality due to balling, excessive spatter, and an augmented gas induced porosity [16]. Therefore, a trade-off must be found.

A popular approach is to regroup multiple operating parameters into one, the volumetric energy density E_d. It is estimated trough the following formula:

$$E_d = \frac{P}{v_s h t}$$

where t is the layer thickness and h is the hatch space. As a rule of thumb, E_d should be chosen in the range between 60 and 75 $[\frac{J}{mm^3}]$ [18]. However, the criterion is insufficient and others phenomena, such as melt pools overlapping, should be considered [21]. Very few studies were carried out to optimize h and t independently. Their values lie generally respectively in the intervals [50 ; 200] $[\mu m]$ and [20 ; 60] $[\mu m]$. It was observed that for t = 30 [μm], an optimal set of parameters values in terms of density is P = 200 [W], $v_s = 1400[\frac{mm}{s}]$ and h = 105 [μm] [11].

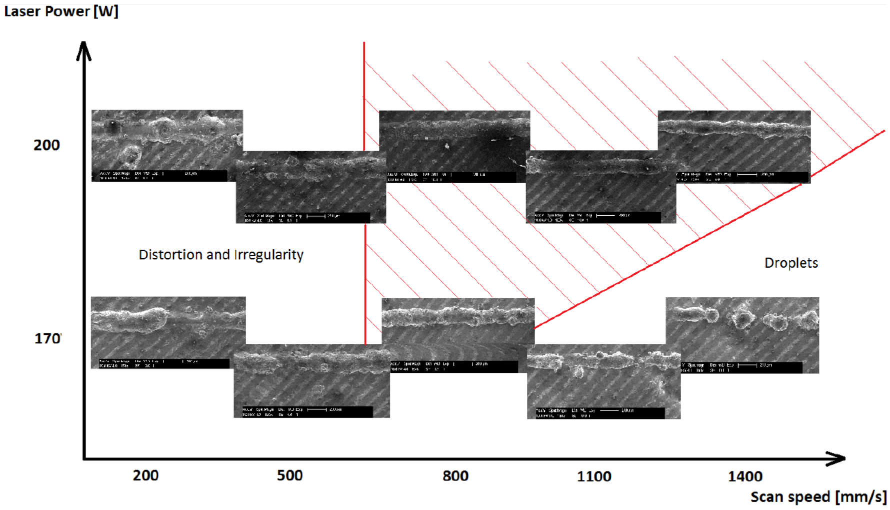

FIGURE 2.4: Process window for SLM of AlSi10Mg, based on the top view of single track scans (from Kempen et al, 2011).

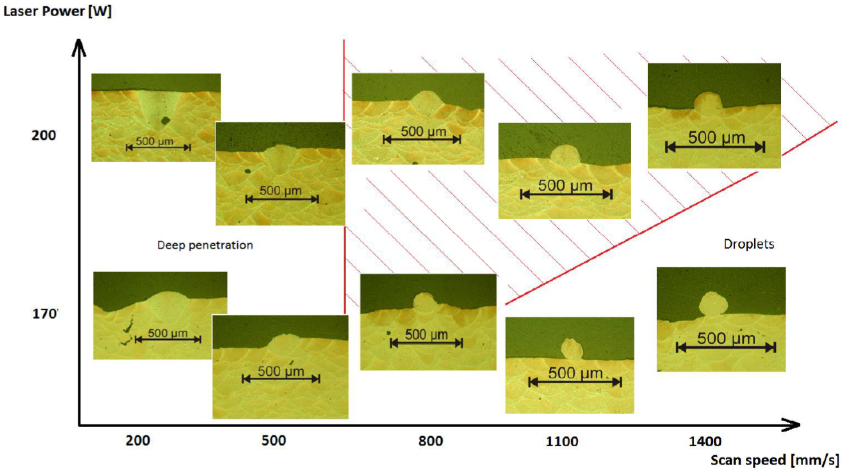

FIGURE 2.5: Process window for SLM of AlSi10Mg, based on the front view of single track scans (from Kempen et al, 2011).

The other process parameters will be covered for the sake of completeness. Let us first look into the particle-related parameters. The particle size D_a of the powder should be as small as possible to ensure a good flowability and allow for thin layers [11]. Typical values stretch from 15 to 60 [μm]. The size distribution is more delicate to outline. On one hand, wider distributions often generate better bed density, parts with higher density and better surface finish. On the other hand, narrower ones usually provide better flowability and parts with better strength and hardness [15]. In most cases, a middle ground between the two should be sought. In SLM applications, powder is often successively recycled multiple times. This leads to their progressive contamination with moisture, which causes an increase of hydrogen porosity in the produced parts [23]. The problem can be overcome by drying the powder or using fresh one. Unfortunately - in the case of aluminium alloys - no findings were made regarding the prediction of a threshold at which one should take action [4].

The choice of scan pattern has great importance. There exist a few different strategies. The common ones use unidirectional, bidirectional or islands patterns (see figure 2.6). The scan direction(s) should always be rotated between successive layers to favorise isotropy, especially in the unidirectional case since it causes height variations along a layer [2]. The islands pattern is based on a decomposition in small domains with short scanning tracks. Two usual strategies can be distinguished among this group: the chessboard and the hexagonal one. A study proved the superiority of an island pattern over a bidirectional one in terms of both ultimate tensile stress σ_u and strain at fracture ϵ_f for a 316L stainless steel-Inconel 718 material [25]. It was also shown that it was possible to fabricate pure titanium samples without cracks using an island pattern, and not with a bidirectional one [13]. This is seemingly due to the greater accumulation of internal stresses and to the weaker interlayer bounding of the second case.

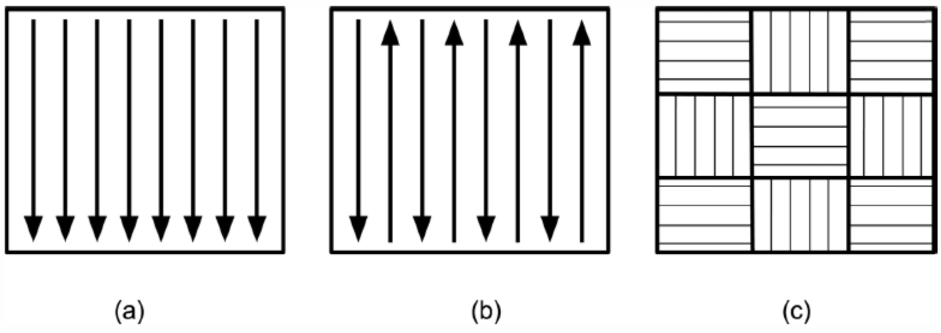

FIGURE 2.6: Schematic representation of scanning strategies commonly used in LSM (a) unidirectional long scan track; (b) bidirectional long scan track, and (c) islands (from Mertens et al, 2017).

Furthermore, dual scanning strategies were proven to be effective. For example, a pre-scan with low E_d can flatten the powder bed before it is consolidated, which leads to a reduction of porosity [16]. It was also shown that scanning the contour of the part being built at lower E_d can better the surface roughness for AlSi12Mg [17]. One should note too that the final properties of the fabricated part can strongly depend on the building direction (see figure 2.7) [7].

Other laser-related parameters - the spot size and the pulse properties - can also influence the process. Only the laser spot size at the 99% contour $\phi_{99\%}$ is frequently cited in literature. Its value lies between 100 and 200 $[\mu m]$.

Finally, the temperature of the powder bed and feeder affect the final properties of the fabricated parts as well. In particular, it was observed that pre-heating the powder at 300° C mitigates the differences of fatigue resistance between tensile specimens built in different directions: it is possible that the slower cooling rate induced helps reducing the distortions and internal stresses [5].

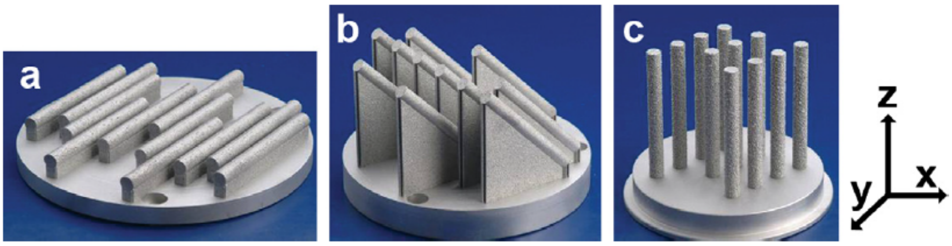

FIGURE 2.7: Samples (static tensile) built in different directions: (a) 0°, (b) 45°, and (c) 90° (from Brandl et al, 2012).

Comparer les résultats avec alliage coulé/forgé

Once the porosity problem is sorted out, other matters can be addressed such as productivity and surface roughness. The latter is problematic as the surface finish obtained with SLM is typically of such poor quality that all cracks initiate near the surface for a sample with relative density $\rho_{rel} > 99\%$ [5]. As said before, it is possible to reduce the surface roughness by mean of a dual scan strategy. However, the only options to obtain significantly better surface finish is currently to machine or polish the fabricated parts. This is one of the main weak points of SLM.

2.4 Post treatments

Post-traitements dont traitements thermiques, sur lesquels on se focalise. Expliquer

Chapter 3

Materials and methods

Description expériences et machines

3.1 Powder follow-up

3.1.1 Sieving

3.1.2 Grain size and distribution

3.1.3 Composition

3.2 Fabrication process parameters

The same direct metal printer (DMP) was used to fabricate all specimens throughout this work. It is a *ProX DMP 200* printer, manufactured by *3D Systems* (see figure 3.1). It uses a laser with a theoretical maximal power of 300 [W] and wavelength $\lambda = 1070$ [nm] [1]. Its actual maximal power is $P_{max} = 273.6[W]$. [QUEL EST LE SPOT SIZE?] The maximal envelope capacity of the machine (W x D x H) is 140 x 140 x 125 [mm]. Its typical accuracy is +/- 50 [μm] for small parts and +/- 0.2% for large parts. It allows for the set-up of a protection atmosphere. However, it does not integrate any heating feature for the build bed.

In this thesis, argon was used as shielding gas. The composition of the gas environment was monitored so as to keep $p_{O2} < 500$ [ppm]. Laser compensations were set to take into account the excess energy at the start and end of the scanning vectors (see figure 3.2). These were chosen in accordance with the manufacturer recommendations (figure 3.3). Values for h and t were respectively set to 100 [μm] and 30 [μm]. The other process parameters were varied so as to optimize the properties of the built specimens. Educated guesses were made based on literature and previous works done at the UCL. The parameters used are resumed in annex A.1. Batches were named in the format X200-*yymmdd*. The prefix "X200" refers to the DMP used. It is followed by the date of printing (6 digits). Recycled powder was used for every batch except for X200-180222 and X200-180228. In the case of samples with contour scanning strategy, the contours were pre scanned for each powder layer with the same P and v_s used for the bulk.

All batches were first prepared on *DMP ProX Manufacturing*, a dedicated CAD software. It enabled to chose the values for the parameters previously mentioned, as well as the position of the specimens. The scanning order was automatically chosen. Figures with detailed specimens positions, denominations, scanning orders and sintering durations are available in annex A.2.

FIGURE 3.1: ProX DMP 200 printer (from the user's ProX DMP 200 general instructions document).

An island scanning strategy was chosen on account of research done on the subject (see section 2.3). It is a hexagonal pattern with ??? [OVERLAP? TAILLE DES HEXAGONES?]

Insérer images de trajets du laser.

[Parler des éprouvettes utilisées]

3.3 Heat treatments

The heat treatments were conducted inside a unique oven of the ... model, manufactured by ..., which is able to reach a temperature of 400° C. Samples temperature data was obtained through a thermocouple welded to the sample surface. [Méthode de soudage, élévation de la température durant l'opération] The data was displayed and saved every 10 seconds, with a precision of 0.1° C, thanks to a ..., connected to the thermocouple (see Fig. for both devices).

Samples that were subject to a heat treatment were named in a particular format, to ease distinction between them. They received the name of the batch, followed by "TT-*holdingtemperature-holdingtime-specific conditions*".

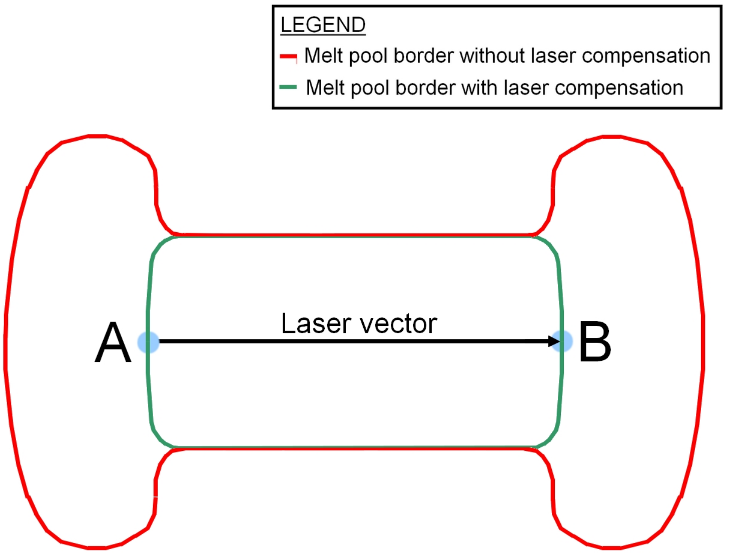
LEGEND
🟥 Melt pool border without laser compensation
🟩 Melt pool border with laser compensation
A
Laser vector
B

FIGURE 3.2: Melt pool contours with and without laser compensation (exaggeration).

3.4 Characterisation

3.4.1 Density

Hydrostatic weighing

Multiple methods were considered to estimate the relative density of the fabricated specimens. The first one is hydrostatic weighting (also called hydrodensitometry). It is a direct application of the well-known Archimedes' principle, which can be stated as follows: " When a body is (partially or totally) immersed in a fluid, the upthrust on the body is equal to the weight of fluid displaced." [6]. By weighing each pieces in air and in water - giving respectively values of dry weight W_a and underwater weight W_w - one can calculate the apparent density ρ_a [10]:

$$\rho_a = \frac{W_a}{W_a - W_w} \cdot \rho_w$$

where ρ_w is the water density. The apparent relative density $\rho_{a,rel}$ of the specimens can then be calculated with:

$$\rho_{a,rel} = \frac{\rho_a}{\rho_b}$$

where $\rho_b = 2.68[\frac{g}{mm^3}]$ is the theoretical bulk density of AlSi10Mg [19]. All weightings were done with a *Sartorius BP121S* analytical balance with precision of 0.1 [mg] [20]. Samples were immersed in demineralised water for more than twelve hours before the measurements to impregnate them. The weightings were also done in demineralised water. Water temperature was measured with a precision glass thermometer to compute ρ_w as accurately as possible thanks to tabulated values [22]. Multiple measurements were done for each sample in order to increase the method's reliability.

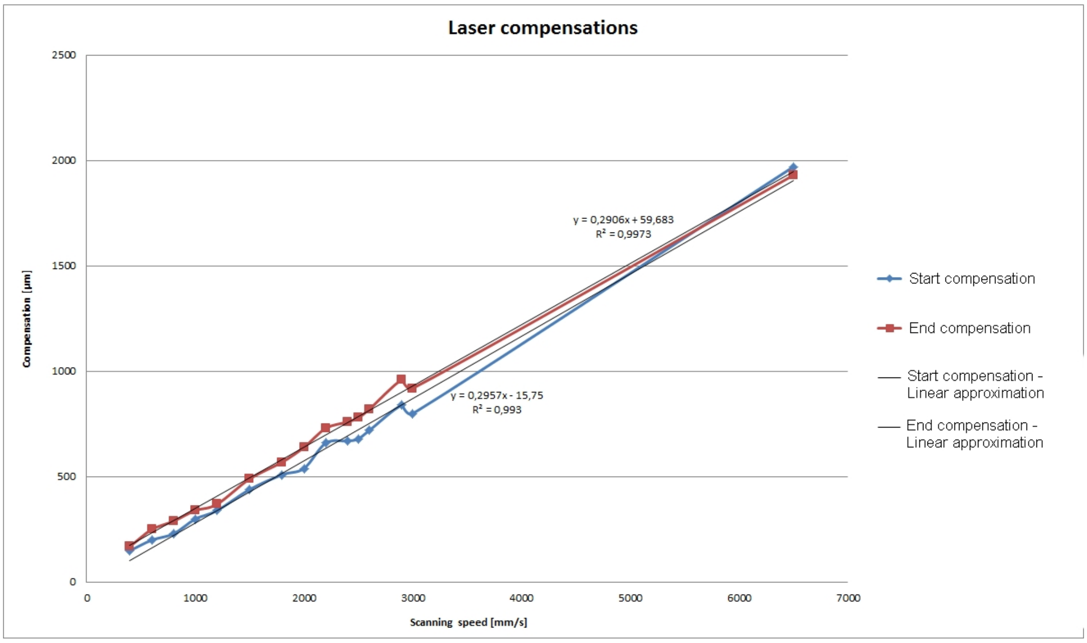

FIGURE 3.3: Laser compensations as a function of the scanning speed (as recommended by the manufacturer).

The technique was employed with "as-built" and polished cubes. This second option reduces the risks of air trapping by the surface roughness, which can distort the results (by overestimating the closed porosities volume). A mettre dans la discussion en fait peut-être? All six faces of the tested cubes were polished with P320 silicon carbide sandpaper sheets and briefly with P1200 ones.

Relative optical density image analysis

Another method was used to estimate the relative density of the various samples: the relative optical density image analysis (RODIA). For this purpose, the samples were cut with a micro-cutting machine and underwent the polishing routine detailed in table 3.1. Pictures of the polished sections were then taken under the optical microscope.[Infos sur le microscope, grossissement] The pictures were taken with a *Huawei Mate 10 Lite* smart-phone trough the lens of the microscope. The used camera has a resolution of 16 [MP]. This option was chosen over the camera directly connected to the microscope, since it only has 5 [MP] resolution.

With the help of the *ImageJ* software, the surface of both the porosities and the whole surface could be isolated for each analysed image (see figure 3.4). The surface fraction occupied by porosities could then be obtained as the ratio between the areas of the two (in pixels). If we approximate that the porosities surface fraction is equal to the volumetric one, that method gives an estimation of the relative density ρ_{rel}.

The images isolations in "foregrounds" and "backgrounds" were done trough manual thresholding based on pixel intensity quantifications. An optimal threshold

Step	Polishing surface	Abrasive	Grain size	Lubricant type	Rotation speed [rpm]
1	MD-piano 220	Diamond	P220	Water	200-300
2	MD-piano 1200	Diamond	P1200	Water	200-300
3	MD-largo	DP-spray	9 μm	Alcohol	150
4	DP-DAC	DP-spray	3 μm	Alcohol	150
5	DP-NAP	DP-spray	1 μm	Alcohol	150

TABLE 3.1: Polishing routine for Al-Si alloys

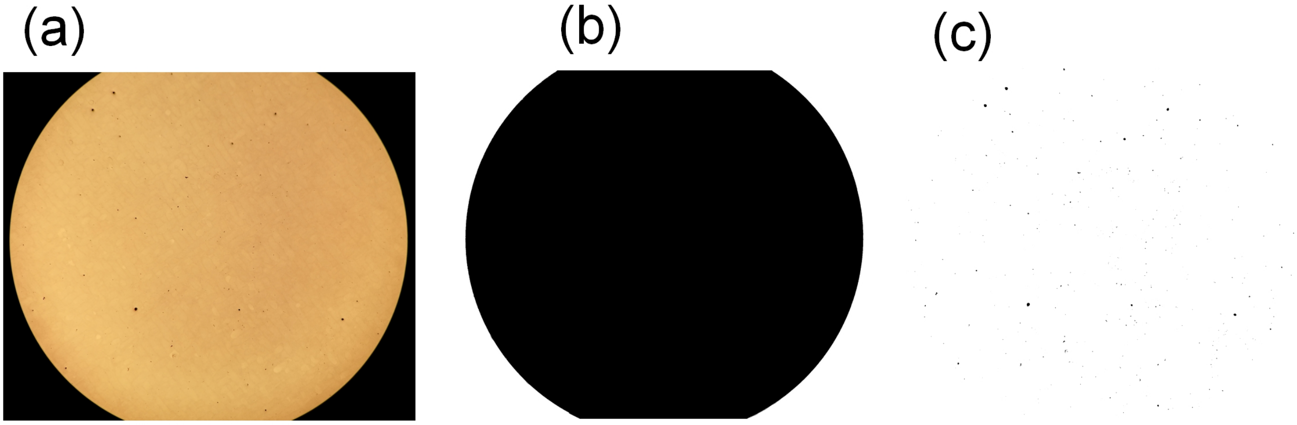

FIGURE 3.4: RODIA procedure for specimen X200-180319-cub 1: (a) Original picture of polished section (b) Whole surface isolation with *ImageJ* (c) Porosities isolation with *ImageJ*.

was sought for porosities isolation so as to include only holes, and as many as possible. Particular attention was given to the photography in order to obtain the best contrast, focus and intensity homogeneity.

3.4.2 Microscopy

Scanning electron microscopy

Optical microscopy

Mesures Taille de bains

3.4.3 Composition

3.4.4 Mechanical properties

Hardness test

Vickers hardness measurements were made with a *Wolpert Dia-Testor 2RC* tester. All analysed specimens were previously cut with a micro-cutting machine for the purpose of observing their bulk hardness. For each test, a pyramidal indenter (see figure 3.5) was pressed on the samples surfaces with a load of 10 [kg] during 10 [sec]. The indentation durations were measured with a digital timer and the tests were stopped manually. The two diagonals lengths of the resulting indents were then evaluated using a ruler on the screen of the machine, which displays an image of the sample's surface captured by an embedded optical microscope.

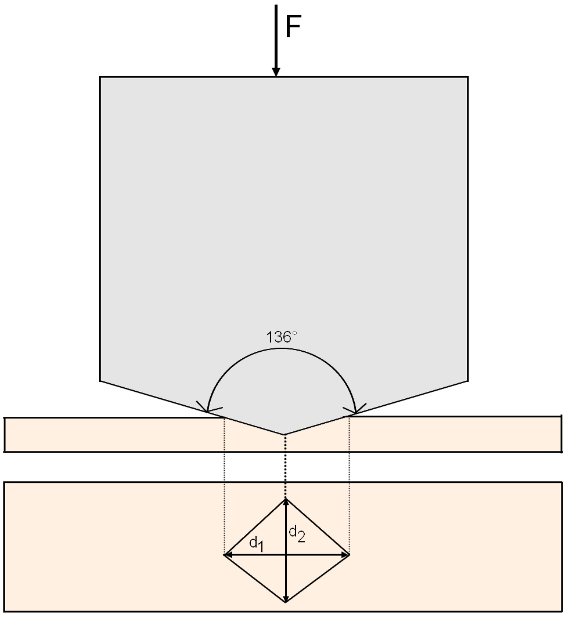

FIGURE 3.5: Schematization of the Vickers harness test

Multiple tests were made for every samples and the mean diagonal length value was computed for each test. The corresponding Vickers harness values HV could then be found using a conversion table.

Traction test

Chapter 4

Results

Analyses statistiques etc...

4.1 Parameters optimisation

4.2 Reproducibility

4.3 Powder ageing

4.3.1 Grain size and distribution

4.3.2 Composition

Fresh powder

Recycled powder

Date of sampling	Date of last addition of fresh powder	Composition [%wt]			
		Al	Fe	Mg	Si
23/10/2017	07/09/2017	89.2	0.12	0.49	10.2
09/01/2018	07/09/2017	89.3	0.13	0.48	10.1
12/01/2018	07/09/2017	89.4	0.13	0.48	10
21/02/2018	07/09/2017 OU POUDRE NEUVE?	89.1	0.19	0.51	10.3
13/03/2018	22/02/2018	89.1	0.16	0.51	10.1

TABLE 4.1: Composition of recycled AlSi10Mg powder as a function of the date

4.4 Heat treatments

4.5 Mechanical testing

Chapter 5

Discussion

Que conclure d'après les résultats?

5.1 Parameters optimisation

5.2 Reproducibility

5.3 Powder ageing

5.3.1 Grain size and distribution

5.3.2 Composition

5.4 Density measures assessments

5.5 Heat treatment optimisation

Chapter 6

Conclusion

They incorporate in a synthetic way the main results and compare them with the initial objectives. Generally, this final chapter also presents prospects for the continuation of the work undertaken.

Appendix A

Batches fabrication details

A.1 Process parameters

Dimensions of the cubic and cylindrical specimens are noted in accordance with figure A.1. [AJOUTER DERNIER BATCH]

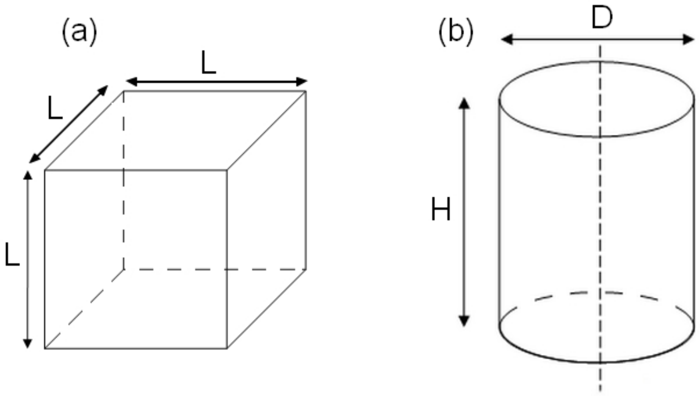

FIGURE A.1: Dimensions notations for (a) cubic specimens (b) cylindrical specimens

A.2 Specimens positioning, fabrication orders and sintering times

A.2.1 Batch X200-171024

A.2.2 Batch X200-180109

... ...

A.2.3 ...Other batches

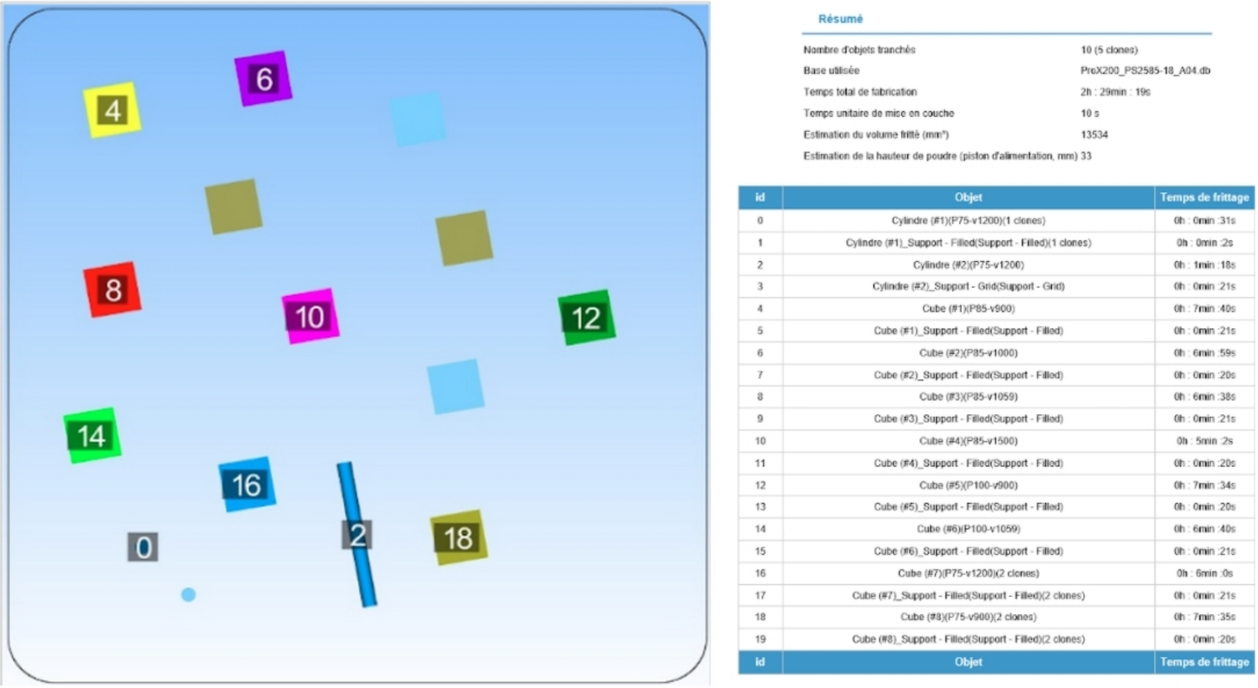

Résumé

Nombre d'objets tranchés	10 (5 clones)
Base utilisée	ProX200_PS2585-18_A04.db
Temps total de fabrication	2h : 29min : 19s
Temps unitaire de mise en couche	10 s
Estimation du volume fritté (mm³)	13534
Estimation de la hauteur de poudre (piston d'alimentation, mm)	33

id	Objet	Temps de frittage
0	Cylindre (#1)(P75-v1200)(1 clones)	0h : 0min :31s
1	Cylindre (#1)_Support - Filled(Support - Filled)(1 clones)	0h : 0min :2s
2	Cylindre (#2)(P75-v1200)	0h : 1min :18s
3	Cylindre (#2)_Support - Grid(Support - Grid)	0h : 0min :21s
4	Cube (#1)(P85-v900)	0h : 7min :40s
5	Cube (#1)_Support - Filled(Support - Filled)	0h : 0min :21s
6	Cube (#2)(P85-v1000)	0h : 6min :59s
7	Cube (#2)_Support - Filled(Support - Filled)	0h : 0min :20s
8	Cube (#3)(P85-v1059)	0h : 6min :38s
9	Cube (#3)_Support - Filled(Support - Filled)	0h : 0min :21s
10	Cube (#4)(P85-v1500)	0h : 5min :2s
11	Cube (#4)_Support - Filled(Support - Filled)	0h : 0min :20s
12	Cube (#5)(P100-v900)	0h : 7min :34s
13	Cube (#5)_Support - Filled(Support - Filled)	0h : 0min :20s
14	Cube (#6)(P100-v1059)	0h : 6min :40s
15	Cube (#6)_Support - Filled(Support - Filled)	0h : 0min :21s
16	Cube (#7)(P75-v1200)(2 clones)	0h : 6min :0s
17	Cube (#7)_Support - Filled(Support - Filled)(2 clones)	0h : 0min :21s
18	Cube (#8)(P75-v900)(2 clones)	0h : 7min :35s
19	Cube (#8)_Support - Filled(Support - Filled)(2 clones)	0h : 0min :20s
id	Objet	Temps de frittage

FIGURE A.2: Specimens positions, order of fabrication and sintering times for batch X200-171024

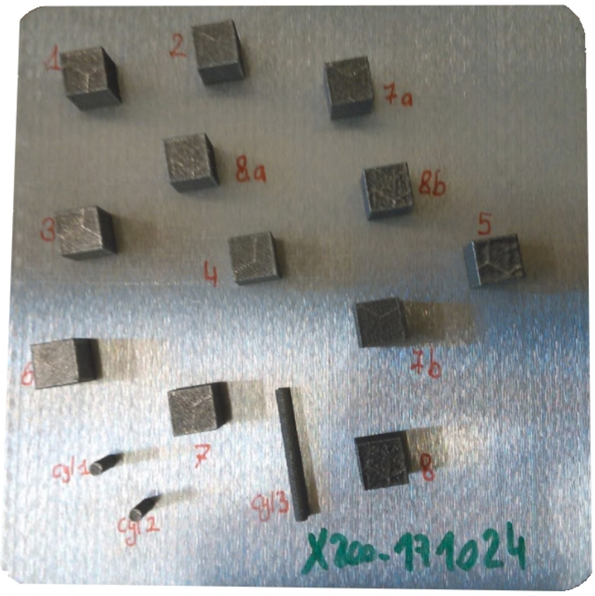

FIGURE A.3: Photography of the manufacturing plate after completion of the fabrication of batch X200-171024

Batch name	Contour	Type	Dimensions [mm]	Specimen name	$\frac{P}{P_{max}}[-]$	$v_s[\frac{mm}{s}]$
X200-171024	No	Cubic	L=10	1	0.85	900
				2		1000
				3		1059
				4		1500
				5	1	900
				6		1059
				7, 7a, 7b	0.75	1200
				8, 8a, 8b		900
X200-180109	No	Cubic	L=10	7c,...7q (15 spec.)	0.75	1200
				8c,...8q (15 spec.)		900
X200-180220	No	Cubic	L=5	TT150-2	0.75	1200
				TT200-2		
				TT300-2		
				TT300-2-plaque		
				TT150-2-real		
				TT200-2-real		
				TT250-2-real		
				TT300-2-real		
X200-180222	No	Cubic	L=10	12	0.75	1200
				13		
X200-180228	Yes	Cylindrical	D=6, H=2	1	0.75	1200
				2		
				3		
X200180313	Yes	Cylindrical	D=6, H=10	1	0.75	1200
				2		
			D=12, H=10	3		
				4		
X200-180319	No	Cubic	L=10	cub 1	0.75	1200
				cub 2		
				cub 3		
				cub 4		
				cub 5		
			L=5	TT300-1-real		
	Yes	Cylindrical	D=6, H=10	cyl 1		
				cyl 2		
			D=12, H=10	cyl 3		
				cyl 4		

TABLE A.1: Process parameters used for the specimens manufacturing

Bibliography

[1] *3D Systems Inc, Direct metal printers: Metal Additive Manufacturing with the ProX^{TM} DMP 3D printers*. 2016. URL: http://sintermedia.gkn.com/blog/the-advantages-of-https://www.3dsystems.com/sites/default/files/2017-01/3D-Systems_DMP_Tech_Specs_USEN_2017.01.23_WEB.pdf (visited on 13/04/2018).

[2] Nesma T. Aboulkhair et al. 'On the formation of AlSi10Mg single tracks and layers in selective laser melting: Microstructure and nano-mechanical properties'. In: *Journal of Materials Processing Tech.* 230.Complete (2016), pp. 88–98.

[3] Nesma T. Aboulkhair et al. 'Reducing porosity in AlSi10Mg parts processed by selective laser melting'. In: *Additive Manufacturing* 1-4 (2014). Inaugural Issue, pp. 77 –86. URL: http://www.sciencedirect.com/science/article/pii/S2214860414000062.

[4] Nesma T. Aboulkhair et al. 'Selective laser melting of aluminum alloys'. In: *MRS Bulletin* 42.4 (2017), 311–319.

[5] Erhard Brandl et al. 'Additive manufactured AlSi10Mg samples using Selective Laser Melting (SLM): Microstructure, high cycle fatigue, and fracture behavior'. In: *Materials & Design* 34 (2012), pp. 159 –169. URL: http://www.sciencedirect.com/science/article/pii/S0261306911005590.

[6] John Daintith. *A Dictionary of Physics*. Oxford University Press, 2009. URL: http://www.oxfordreference.com/view/10.1093/acref/9780199233991.001.0001/acref-9780199233991.

[7] Pauline Delroisse et al. 'Effect of strut orientation on the microstructure heterogeneities in AlSi10Mg lattices processed by selective laser melting'. In: *Scripta Materialia* 141 (2017), pp. 32 –35. ISSN: 1359-6462.

[8] Christian Haase et al. 'Exploiting Process-Related Advantages of Selective Laser Melting for the Production of High-Manganese Steel.' In: *Materials* 10(1).56 (2017).

[9] Simon Hoeges. *Additive manufacturing technologies: 6 Unique Benefits Of Selective Laser Melting*. 2017. URL: http://sintermedia.gkn.com/blog/the-advantages-of-selective-laser-melting (visited on 12/04/2018).

[10] Frank I. Katch. 'Apparent Body Density and Variability during Underwater Weighing'. In: *Research Quarterly. American Association for Health, Physical Education and Recreation* 39.4 (1968), pp. 993–999. URL: https://shapeamerica.tandfonline.com/doi/abs/10.1080/10671188.1968.10613450.

[11] Karolien Kempen et al. 'Microstructural analysis and process optimization for selective laser melting of AlSi10Mg'. In: *Solid Freeform Fabrication Symposium Proceedings* (2011). Conference paper, pp. 484–495. URL: https://sffsymposium.engr.utexas.edu/Manuscripts/2011/2011-37-Kempen.pdf.

[12] K.-H. Leitz et al. 'Multi-physical simulation of selective laser melting'. In: *Metal Powder Report* 72.5 (2017), pp. 331 –338. URL: `http://www.sciencedirect.com/science/article/pii/S0026065716300200`.

[13] Xiao Peng Li et al. 'Tailoring Commercially Pure Titanium Using Mo2C During Selective Laser Melting'. In: *Solid Freeform Fabrication 2017: Proceedings of the 28th Annual International* (Aug. 2017). Conference paper, pp. 160–166.

[14] Rene Lippert and Roland Lachmayer. 'A Design Method for SLM-Parts Using Internal Structures in an Extended Design Space'. In: (Sept. 2018), pp. 14–23.

[15] Bochuan Liu et al. 'Investigaztion the effect of particle size distribution on processing parameters optimisation in selective laser melting process'. In: (Jan. 2011). Conference paper, pp. 227–238.

[16] Anne I. Mertens, Jocelyn Delahaye and Jacqueline Lecomte-Beckers. 'Fusion-Based Additive Manufacturing for Processing Aluminum Alloys: State-of-the-Art and Challenges'. In: *Advanced Engineering Materials* 19.8 (2017), p. 1700003. URL: `https://onlinelibrary.wiley.com/doi/abs/10.1002/adem.201700003`.

[17] K.G. Prashanth, S. Scudino and J. Eckert. 'Defining the tensile properties of Al-12Si parts produced by selective laser melting'. In: *Acta Materialia* 126 (2017), pp. 25 –35. URL: `http://www.sciencedirect.com/science/article/pii/S135964541630982X`.

[18] Noriko Read et al. 'Selective laser melting of AlSi10Mg alloy: Process optimisation and mechanical properties development'. In: *Materials & Design (1980-2015)* 65 (2015), pp. 417 –424. URL: `http://www.sciencedirect.com/science/article/pii/S0261306914007468`.

[19] *Renishaw plc, AlSi10Mg-0403 powder for additive manufacturing data sheet*. 2015. URL: `file:///E:/Downloads/H-5800-1061-01-A_AlSi10Mg-0403_400_W_material_data_sheet.pdf` (visited on 15/04/2018).

[20] *Sartorius AG, Sartorius BP121S Installation And Operating Instructions Manual*. 2000. URL: `https://www.manualslib.com/products/Sartorius-Bp121s-3748053.html` (visited on 15/04/2018).

[21] Ming Tang, P. Chris Pistorius and Jack L. Beuth. 'Prediction of lack-of-fusion porosity for powder bed fusion'. In: *Additive Manufacturing* 14 (2017), pp. 39 –48. URL: `http://www.sciencedirect.com/science/article/pii/S2214860416300471`.

[22] Robert C Weast. *CRC Handbook of Chemistry and Physics 53rd Edition*. CRC Press, 1973. URL: `http://jupiter.plymouth.edu/~jsduncan/courses/2012_Spring/Techniques/Exams/DensityOfWater-vs-Temp.pdf`.

[23] Christian Weingarten et al. 'Formation and reduction of hydrogen porosity during selective laser melting of AlSi10Mg'. In: *Journal of Materials Processing Technology* 221 (2015), pp. 112 –120. URL: `http://www.sciencedirect.com/science/article/pii/S0924013615000564`.

[24] Chor Yen Yap et al. 'Review of selective laser melting: Materials and applications'. In: 2 (Dec. 2015), p. 041101.

[25] Yan Zhou et al. 'Investigation on the scan strategy and property of 316L stainless steel-Inconel 718 functionally graded materials fabricated by selective laser melting'. In: *The Proceedings of the 26th Solid Freeform Fabrication Symposium* (Aug. 2015). Conference paper, pp. 700–707.